Pushing the boundaries of chemistry?
It takes #HumanChemistry

Make your curiosity and talent as a chemist matter to the world with a specialty chemicals leader. Together, we combine cutting-edge science with engineering expertise to create solutions that answer real-world problems. Find out how our approach to technology creates more opportunities for growth, and see what chemistry can do for you at:

evonik.com/career

EVONIK
Leading Beyond Chemistry

Emissive Charge-Transfer States at Hybrid Inorganic/Organic Heterojunctions Enable Low Non-Radiative Recombination and High-Performance Photodetectors

Flurin Eisner,* Georgie Foot, Jun Yan, Mohammed Azzouzi, Dimitra G. Georgiadou, Wai Yu Sit, Yuliar Firdaus, Guichuan Zhang, Yen-Hung Lin, Hin-Lap Yip, Thomas D. Anthopoulos, and Jenny Nelson*

Hybrid devices based on a heterojunction between inorganic and organic semiconductors have offered a means to combine the advantages of both classes of materials in optoelectronic devices, but, in practice, the performance of such devices has often been disappointing. Here, it is demonstrated that charge generation in hybrid inorganic–organic heterojunctions consisting of copper thiocyanate (CuSCN) and a variety of molecular acceptors (ITIC, IT-4F, Y6, $PC_{70}BM$, C_{70}, C_{60}) proceeds via emissive charge-transfer (CT) states analogous to those found at all-organic heterojunctions. Importantly, contrary to what has been observed at previous organic–inorganic heterojunctions, the dissociation of the CT-exciton and subsequent charge separation is efficient, allowing the fabrication of planar photovoltaic devices with very low non-radiative voltage losses (0.21 ± 0.02 V). It is shown that such low non-radiative recombination enables the fabrication of simple and cost-effective near-IR (NIR) detectors with extremely low dark current (4 pA cm^{-2}) and noise spectral density (3 fA $Hz^{-1/2}$) at no external bias, leading to specific detectivities at NIR wavelengths of just under 10^{13} Jones, close to the performance of commercial silicon photodetectors. It is believed that this work demonstrates the possibility for hybrid heterojunctions to exploit the unique properties of both inorganic and organic semiconductors for high-performance opto-electronic devices.

1. Introduction

An interesting alternative to all-organic optoelectronic devices is a hybrid device comprising both organic and inorganic materials in a heterojunction, in which the advantageous properties of both types of material can be combined. In particular, such hybrid heterojunctions offer the possibility of combining visible-light absorbing organic semiconductors, which tend to have narrow-bandwidth absorption spectra that can be spectrally tuned to suit specific applications, with high dielectric constant crystalline inorganic semiconductors.[1,2] This pairing is of specific interest because the high dielectric permittivity and crystallinity of the inorganic phase are thought to be beneficial for efficient dissociation of photoexcited excitons at the interface, and hence allow for the fabrication of devices with high charge photogeneration efficiency in response to visible light.[3–7] It has been suggested that

F. Eisner, G. Foot, J. Yan, M. Azzouzi, D. G. Georgiadou, W. Y. Sit, J. Nelson
Department of Physics
Imperial College London
South Kensington, London SW7 2AZ, UK
E-mail: f.eisner15@imperial.ac.uk; jenny.nelson@imperial.ac.uk

D. G. Georgiadou
Centre for Electronics Frontiers
Electronics and Computer Science
University of Southampton
Southampton SO17 1BJ, UK

Y. Firdaus, T. D. Anthopoulos
Division of Physical Sciences and Engineering and KAUST Solar Centre
King Abdullah University of Science and Technology (KAUST)
Thuwal 23955–6900, Saudi Arabia

The ORCID identification number(s) for the author(s) of this article can be found under https://doi.org/10.1002/adma.202104654.

Y. Firdaus
Research Center for Electronics and Telecommunication
Indonesian Institute of Science
Jalan Sangkuriang Komplek LIPI Building 20 level 4, Bandung 40135, Indonesia

G. Zhang
Institute of Polymer Optoelectronic Materials and Devices
State Key Laboratory of Luminescent Materials and Devices
South China University of Technology
Guangzhou 510640, P. R. China

Y.-H. Lin
Department of Physics
University of Oxford
Parks Road, Oxford OX1 3PU, UK

H.-L. Yip
Department of Materials Science and Engineering
City University of Hong Kong
Tat Chee Avenue, Kowloon, Hong Kong

the high dielectric constant and delocalization of free carriers in the crystalline inorganic material might contribute to reducing the free energy that is necessary to efficiently dissociate charge-transfer (CT) excitons at inorganic/organic heterojunctions and that higher open-circuit voltage (V_{oc}) can therefore be achieved for a given optical bandgap in photovoltaic (PV) devices.[4,8] In practice, however, hybrid-heterojunction solar cells and photodetectors have not reached the expected performance,[1,4,8–14] especially compared to their all-organic heterojunction counterparts.[15] A major limitation has been poor efficiency of photoexcited charge transfer from the organic to the inorganic material and subsequent charge separation.[12,16–21]

The most common combinations of inorganic and organic materials in hybrid heterojunction devices thus far have been pairing either metal oxides (e.g., zinc oxide, ZnO, and titanium dioxide, TiO_2) or chalcogenide nanoparticles (e.g., CdSe) with polymers, such as regioregular poly(3-hexylthiophene-2,5-diyl) (P3HT).[3,4,8,9,22] As an example, solar cells fabricated using the prototypical ZnO:P3HT heterojunction[9,22] suffer from high voltage losses and low photocurrents, which has been suggested to be due to the strong binding of electron–hole pairs formed at the ZnO:organic interface,[23] which is in agreement with theoretical work.[24] Similarly poor performance with other metal oxides has been assigned to trap states at the surface of the metal oxides that prevent charge separation.[11,14] Because of these limitations, ZnO:organic solar cells have achieved limited power conversion efficiencies (PCE) of ≈0.5% in a planar heterojunction architecture, or up to 3% in a bulk-heterojunction (BHJ) architecture,[16] and yield photodetectors with low responsivities.[25,26] Similarly, studies on cadmium sulfide (CdS) nanoparticle:polymer and cadmium selenide (CdSe) nanoparticle:polymer blends have found that charge generation following absorption in the organic component results in poor exciton dissociation and high geminate recombination losses, limiting solar cell efficiencies to ≈3–5%,[5,12,27,28] and showing only limited photodetection capabilities.[29]

In order to address the reasons for this poor optoelectronic performance of hybrid solar cells and photodetectors, the mechanisms of charge separation and voltage generation need to be understood in terms of the states involved at the interface between the organic and inorganic materials. In organic heterojunctions, the primary state that dominates charge recombination in the system has been shown to be a CT-state, which arises from a coulombically bound electron–hole pair in which the electron lies in the lowest unoccupied molecular orbital (LUMO) of the electron-acceptor material and the hole lies in the highest occupied molecular orbital (HOMO) of the electron-donor material.[30–32] CT-like excitons, formed at the interface between the inorganic and organic material, have also been reported to play a role in charge generation in various inorganic/organic heterojunctions when the organic material is the primary absorbing material, but there has been limited success to-date in minimizing recombination through such states.[8,9,22,23,33] However, much less attention has been paid to the role of such states in the charge separation mechanisms in hybrid heterojunctions than in organic heterojunction devices; a careful investigation of such states would be useful in clarifying the practical limits to charge separation in such hybrid systems.

One notable exception to this has been hybrid heterojunction consisting of the inorganic semiconductor copper thiocyanate (CuSCN) with organic semiconductors, either in a bilayer[34] or in a pseudo-BHJ architecture.[35–37] For example, we have previously demonstrated that hybrid devices made from CuSCN nanowire structures grown on a CuSCN donor layer and the methanofullerene $PC_{70}BM$, yield PCEs greater than 5% as a result of efficient hole transfer from the HOMO of $PC_{70}BM$ to the valence band (VB) of CuSCN. Whilst these hybrid layers yielded efficient solar cells, the mechanisms of photocurrent generation were not fully investigated in these works, and the use of fullerenes limited the possible absorption and donor:acceptor energetic offset range and thus the utility of such devices. In this work, we demonstrate for the first time that charge separation in a range of CuSCN/organic heterojunctions proceeds via an emissive CT state whose energy follows the energetic offset between the LUMO of the organic semiconductor and the VB of CuSCN, in analogy to all-organic heterojunctions. Additionally, unlike almost all other hybrid heterojunctions reported thus far, charge generation is efficient due to facile dissociation of photogenerated CT-excitons at the interface. Indeed, we demonstrate high internal quantum efficiencies (>70%) and low non-radiative voltage losses (down to 0.21 V) in solar cells, on par with those achieved by all-organic heterojunctions . We show that this enables the fabrication of near-infrared (NIR) photodetectors with low dark saturation current and noise spectral densities, leading to NIR-specific detectivities that are amongst the highest reported for any organic-semiconductor-based photodetector.

2. Origin of Charge Generation

We begin by studying the nature of charge generation at such a heterojunction to determine whether sufficient photocurrent can be generated to make them viable in optoelectronic devices. The energy levels of CuSCN, an intrinsically p-type inorganic semiconductor, are depicted in **Figure 1**A, showing that its ionization potential (IP) is located at an appropriate energy (−5.4 eV, measured by air photoemission spectroscopy (Figure S1, Supporting Information)) for CuSCN to form a type-II heterojunction with a wide range of small-molecule acceptors; most such acceptor molecules studied for organic PV applications have IP deeper than −5.5 eV and bandgaps of less than 2 eV.[38] As an example, we therefore initially choose the archetypal small-molecule non-fullerene acceptor 3,9-bis(2-methylene-(3-(1,1-dicyanomethylene)-indanone))-5,5,11,11-tetrakis(4-hexylphenyl)-dithieno[2,3-d:2′,3′-d′]-s-indaceno[1,2-b:5,6-b′] dithiophene (ITIC) as the n-type partner of the heterojunction, due to its strong absorption in the visible and HOMO level in the region of −5.5 to −5.6 eV,[39,40] which enables it to form a type-II heterojunction with CuSCN with an appropriate energetic offset for hole transfer from the ITIC HOMO to the VB of CuSCN. A hybrid heterojunction is fabricated by the sequential deposition of CuSCN and ITIC; due to the insolubility of CuSCN in most organic solvents, deposition of the organic layer on top of CuSCN allows for the fabrication of a well-defined (<10 nm root-mean-square roughness, Figure S2, Supporting Information) heterojunction.[34,36]
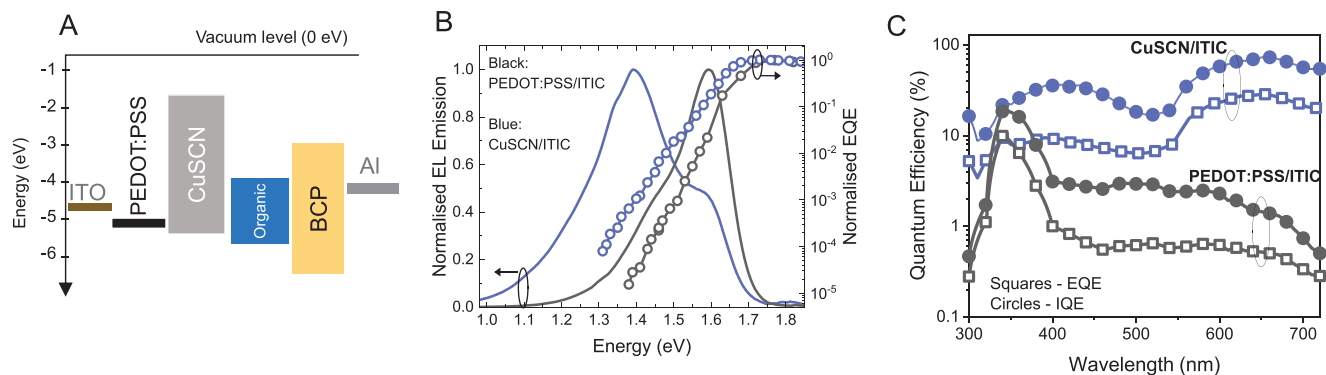
Figure 1. A) Energy levels (materials not in contact with each other) of CuSCN and a typical acceptor-type small organic semiconductor molecule (ITIC), and of the electrodes. Bathocuproine is used as the electron-transport layer. A CT state may be formed between an electron in the LUMO of ITIC and a hole in the VB of CuSCN when the materials are in contact. B) Normalized EL (solid lines) and EQE (symbols and lines) spectra of a CuSCN/ITIC (30 nm) heterojunction, and of an ITIC-only device, where CuSCN was replaced with PEDOT:PSS. C) EQE (open squares) and IQE (closed circles) of a CuSCN/ITIC and a PEDOT:PSS/ITIC device.

Figure 1B shows the electroluminescence (EL) spectra and the onset of the external quantum efficiency (EQE) of devices employing a CuSCN/ITIC heterojunction (blue line and symbols), and of ITIC-only devices (red), with the thickness of ITIC films being 30 ± 5 nm (the optimized thickness for PV device) in both cases. For the ITIC-only device, we substituted CuSCN with the well-known hole transport layer poly(3,4-ethylenedioxythiophene) polystyrene sulfonate (PEDOT:PSS), which we have previously shown does not facilitate charge separation in a heterojunction with $PC_{70}BM$.[35,37] The EL spectrum of PEDOT:PSS/ITIC shows exclusively excitonic emission from ITIC, with a main (0–1) peak centered at ≈1.59 eV, and a shoulder peak centered at ≈1.46 eV, in accordance with previous studies.[41–43] By contrast, the EL emission of CuSCN/ITIC is dominated by a new peak appearing at an energy of ≈1.39 eV, whilst the ITIC excitonic emission is present but strongly quenched. Changing the ITIC thickness does not change the energy of the new emission peak (Figure S3, Supporting Information), but the relative intensity of the peak compared to the ITIC excitonic emission peak decreases with increasing ITIC thickness. This strongly suggests that the origin of this new peak is a state at the CuSCN/ITIC interface and is in agreement with the injection dependent spectra (Figure S4, Supporting Information); additionally, the high intensity of the emission from lower energy states suggests that those states are emissive CT states rather than trap states, since traps would act primarily as non-radiative pathways for recombination.[44]

Similar to the emission spectrum, the sub-bandgap absorption below 1.7 eV (measured as EQE spectrum) of pure ITIC in Figure 1B shows a steep absorption edge, whereas the CuSCN/ITIC sub-bandgap absorption shows a more extended, shallow absorption tail that extends beyond the absorption tail of ITIC to 1.3 eV. The spectral overlap of the bilayer emission and absorption spectra suggests that they originate from the same sub-bandgap state which we estimate to lie at ≈1.5 eV from the crossing of normalized EL and EQE spectra;[45] based on the donor VB (−5.4 eV) and acceptor LUMO energy (−3.85 eV),[46] this is also the energy around which we estimated an interfacial CT state to lie. This result

strongly suggests that the emission originates from a state that is an interfacial CT state in nature; to the best of our knowledge this is the first reported CT state at an inorganic/organic heterojunction involving a p-type inorganic semiconductor and an n-type organic semiconductor.

As we have previously noted, the charge separation efficiency in the case of charge transfer from the organic to the inorganic material in most reported hybrid heterojunctions is very low, which has been attributed to various phenomena including the competing formation of triplet states,[47] trap states at the metal oxide interface,[48–50] and high geminate recombination rates of CT excitons at chalcogenide/polymer interfaces.[12,51] Figure 1C shows the measured EQE and the internal quantum efficiency (IQE) calculated therefrom using a transfer matrix model for a CuSCN/ITIC device and a PEDOT:PSS/ITIC device, with a 30 ± 5 nm ITIC layer in both cases.[52] Notably, the IQE of the CuSCN/ITIC device is ≈70% in the region where there is strong absorption in the ITIC layer (550–710 nm), suggesting a high charge-separation efficiency at the CuSCN/ITIC interface. As expected, the IQE of the PEDOT:PSS/ITIC device is negligible at all photon energies due to the absence of an appropriate interface for charge separation, apart from a peak at low wavelengths due to the contribution of weakly bound excitons.

Since a CT-exciton is, by definition, formed by an electron in the LUMO of the acceptor and a hole in the HOMO (or in this case the VB) of the donor, the energy of the CT state correlates to the energetic difference between these two donor and acceptor (D–A) energy levels at organic heterojunctions,[30,53–55] with the same relationship also having been observed at hybrid heterojunctions.[9,22] In order to further confirm that the emission from the CuSCN/ITIC state is indeed of CT character, we additionally fabricated CuSCN bilayer devices with five more organic semiconductors with a range of LUMO energies. The energetics of the six acceptors, C_{70} and C_{60},[56] IT-4F,[57] Y6,[57] $PC_{70}BM$,[57] and ITIC,[58] are shown in **Figure 2**A, displaying a range of LUMO energies from −4.3 (C_{70}) to −3.85 eV ($PC_{70}BM$), all taken from inverse photoemission spectroscopy values from the literature.[46,59] We note here that whilst fullerenes are considered strictly inorganic semiconductors by some

**ADVANCED
SCIENCE NEWS**

www.advancedsciencenews.com

**ADVANCED
MATERIALS**

www.advmat.de

definitions, we count them here among organic acceptors following common usage in the field.[60,61] Figure 2B shows the EL emission of all five CuSCN/organic heterojunctions at low
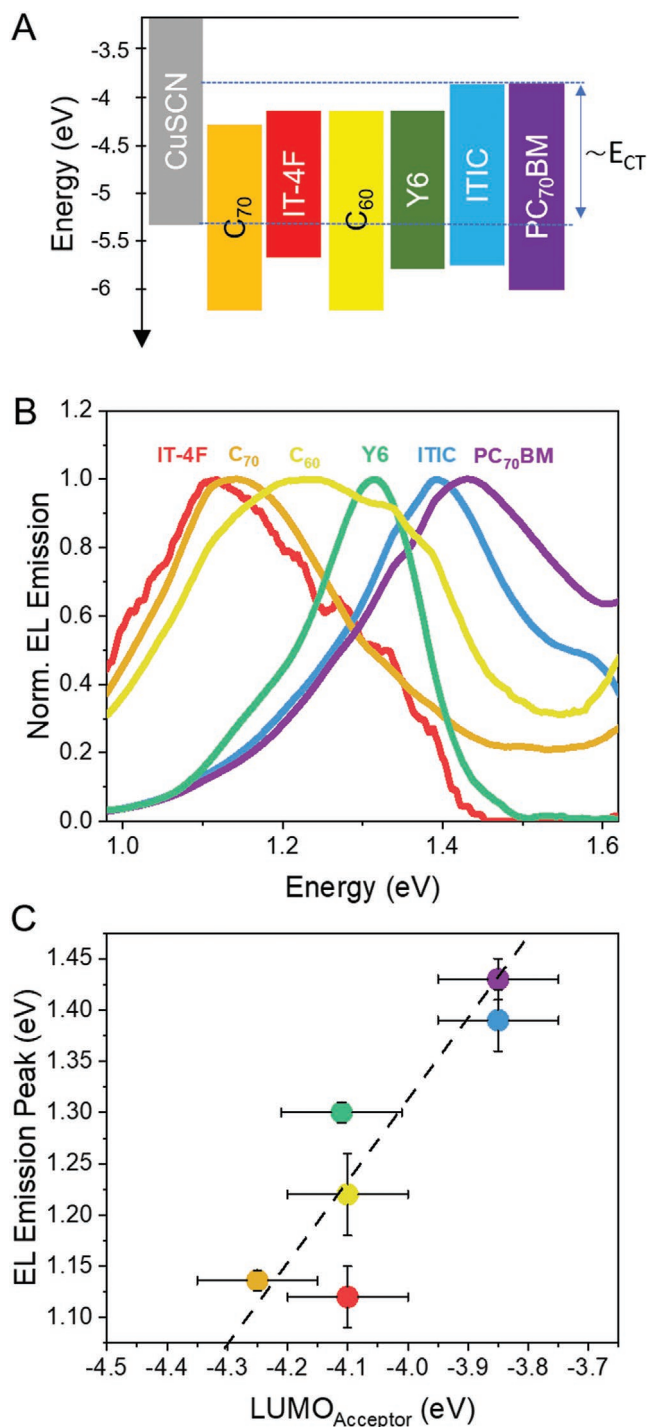

Figure 2. A) Energy levels of CuSCN and small molecules used herein,[46,59] with a E_{CT} value is approximately equal to the difference between the organic LUMO energy and the CuSCN VB, as indicated by the double-headed arrow for CuSCN/PC$_{70}$BM. B) Normalized EL emission spectra of all optimized CuSCN/organic semiconductor bilayer heterojunctions. C) EL emission peak energy plotted as a function of LUMO energy of the organic semiconductor, showing a linear correlation.

injection currents, all of which show emission from a state that is redshifted from the emission of the pristine acceptor (shown in Figure S5, Supporting Information, for clarity), in agreement with the EQE spectra (Figure S7, Supporting Information). As shown by Figure 2C, the energies of the emission peaks show a good positive correlation with the corresponding LUMO of the acceptor whilst being completely uncorrelated with the bandgap of the acceptor (Figure S6, Supporting Information), offering further evidence that the emission peaks originate from an interfacial state at the CuSCN/organic interface, that is, a CT state.

3. Photovoltaic Devices and Voltage Losses

Having established the presence of a CT state at all studied CuSCN/organic heterojunctions, we now present the current density–voltage (J–V) characteristics of optimized devices incorporating these bilayers with optimized organic layer thicknesses (≈ 50 nm for C$_{70}$, 65 nm for C$_{60}$ and 30 nm for ITIC and PC$_{70}$BM, 40 nm for Y6 and IT-4F). The same architecture as in Figure 1A was used for all organic semiconductors, and the J–V characteristics under AM1.5 illumination are shown in **Figure 3**A, with the device characteristics from an average of 8 devices shown in **Table 1**. All devices exhibit a PCE of over 1%, with the best performing device being CuSCN/Y6, which shows a high J_{sc} of over 6 mA cm^{-2}, a V_{oc} of 0.84 V and a PCE of 2.7%. This relatively high photocurrent generation, given the limitation induced by the bilayer architecture, can be attributed to a combination of high absorption coefficient and long-range exciton diffusion in Y6 that has been recently demonstrated using the same system.[34] Interestingly, CuSCN/C$_{70}$ also shows good performance (PCE > 2%) despite the limited spectral range of C$_{70}$ absorption. This can be attributed to a combination of the long-exciton lifetime of C$_{70}$ and its extremely high electron mobility, which we measured to be 2.4 cm^2 V^{-1} s^{-1} using thin-film transistors (Figure S8, Supporting Information). This high mobility is also likely to be partly responsible for the high fill factor (compared to the other devices) of nearly 60% and demonstrates that improved power-conversion-efficiencies may be achievable in bilayer devices if exciton and charge-carrier lifetimes of organic semiconductors can be improved. These performance values are amongst the highest achieved in hybrid bilayer inorganic/organic heterojunctions to date and are surprisingly high given that only one component of the heterojunction contributes to excited-state generation.

We additionally calculated the voltage losses for each device from their EQE and EL spectra using the method of Yao et al.,[62] with the results shown in Table 1 and Figure 3B. As would be expected, devices with fullerene acceptors, characterized by large energetic offsets between the HOMO of the acceptor and the VB of CuSCN, display a high voltage loss due to broadened absorption edge ($\Delta V_{oc,abs}$) due to strong redshift of the CT state absorption compared to the acceptor absorption edge.[63,64] Focusing, therefore, on the two devices with the lowest offsets, CuSCN/ITIC and CuSCN/Y6, it is first noticeable that both have low $\Delta V_{oc,abs}$ of ≈ 0.1 eV, which is comparable to some of the best performing organic BHJ devices,[65,66] although we note that care must be taken when comparing
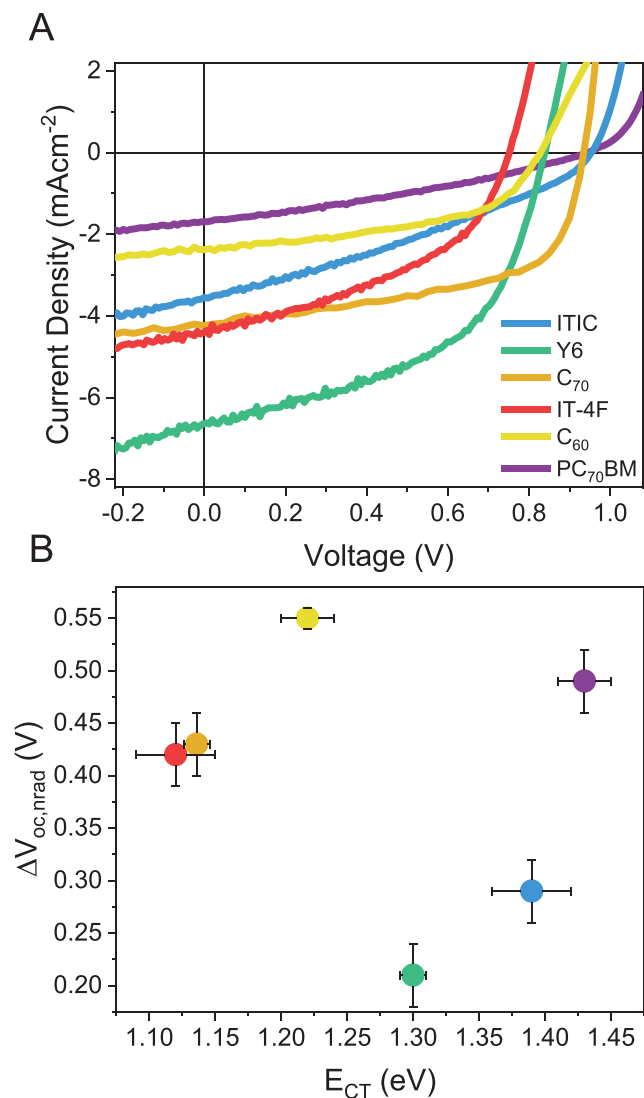
Figure 3. A) *J–V* curves of optimized bilayer devices measured under AM1.5 illumination. B) Non-radiative voltage losses plotted against energy of the CT-state, showing no correlation.

value displayed by CuSCN/Y6, comparable to that of the high efficiency polymer:small-molecule bulk-heterojunction (BHJ) PM6:Y6 blend ($\Delta V_{oc,nrad}$ = 0.23–0.27 V),[65,68] shows that non-radiative recombination pathways in hybrid heterojunction devices can be suppressed with the right choice of materials. Such low non-radiative voltage losses are in agreement with the high magnitude of electroluminescent CT-state emission observed, comparable to the magnitude of CT-state emission from a very well mixed polymer:Y6 bulk-heterojunction device (Figure S10, Supporting Information). Interestingly, plotting the non-radiative voltage losses against the energy of the charge transfer state in Figure 3B, we find no correlation between the two values in the systems studied, which is in agreement with recent work showing an absence of such a correlation in organic solar cells with low energetic offsets between the donor and the acceptor,[69] although we note that the sample size used here may be too small to draw a definite conclusion. Further investigations are required to determine the reasons for the low $\Delta V_{oc,nrad}$ in this system, in comparison to other hybrid heterojunction systems. From a molecular picture of recombination, the factors controlling $\Delta V_{oc,nrad}$ at heterojunctions include reorganisation energy, static dipole moment, density of interface states and the strength of interaction between local excited and CT-states,[41,70] any of which might be affected by the inorganic nature of the donor in this case; this is beyond the scope of this study but merits further investigation. The low non-radiative voltage losses demonstrated suggest that high efficiencies are achievable using CuSCN/organic heterojunctions if, for example, the photocurrent generated can be improved by increasing the area of the CuSCN/organic interface as has been previously demonstrated for CuSCN:PC70BM devices.[36]

It is worth commenting at this point on the fact that based on the properties demonstrated herein (solution processability, evidence of CT state, relatively high open-circuit voltage losses compared to many crystalline inorganic materials), CuSCN appears to display many similar properties to what may be expected of an organic semiconductor. There are, however, important physical and electronic differences that distinguish CuSCN from most organic semiconductors, such as: 1) its VB characteristics, which control the properties relevant for its application as an electron donor (i.e. hole transport and participation in interfacial charge transfer) arise primarily from Cu 3d orbitals,[71–74] as opposed to π orbitals in organic semiconductors; 2) it has a dielectric constant higher than 5[75] (most organic semiconductors have a lower dielectric constant of less than 4; 3) it has high (10^{19} cm^{-3})[72] intrinsic hole concentrations

$\Delta V_{oc,abs}$ between studies since it depends on the definition of the bandgap.[67] Second, both CuSCN/ITIC and CuSCN/Y6 exhibit low non-radiative voltage loss ($\Delta V_{oc,nr}$) values of 0.29 ± 0.2 and 0.21 ± 0.2 eV, respectively. The extremely low

Table 1. Average device characteristics for CuSCN/organic bilayer devices under AM1.5 illumination for a minimum of 5 individual devices, and voltage losses for the best performing device. For clarity, the errors are shown in Table S1, Supporting Information.

Material	J_{SC} [mA cm^{-2}]	V_{oc} [V]	FF [%]	PCE [%]	E_g [eV]	$V_{oc,sq}$ [eV]	$V_{oc,rad}$ [eV]	$\Delta V_{oc,abs}$ [eV]	$\Delta V_{oc,nrad}$ [eV]
C70	4.1	0.94	56	2.2	2.10	1.78	1.36	0.42	0.42
IT-4F	4.2	0.75	44	1.4	1.60	1.32	1.19	0.13	0.43
Y6	6.5	0.84	51	2.8	1.41	1.14	1.05	0.09	0.21
ITIC	3.4	0.94	33	1.1	1.64	1.34	1.23	0.11	0.29
PC70BM	1.3	0.98	45	1.1	2.12	1.81	1.47	0.34	0.49
C60	2.4	0.82	51	1	2.12	1.81	1.37	0.31	0.55

arising from Cu vacancies, amounting to unintentional p doping (most organic semiconductor do not have high intrinsic charge carrier concentrations and are not intentionally or unintentionally doped). We believe, therefore, that the reasons for why CuSCN can be used to fabricate hybrid heterojunctions with similar characteristics to all-organic heterojunctions are intriguing and warrant further investigation in future works.

4. Application as NIR Photodetectors

The simplicity of the device architecture, the low material cost of CuSCN ($0.7 per gram)[76] compared to conventional polymer donors (e.g., P3HT, $400 per gram),[77] and the potentially greater stability due to the absence of a mixed morphology, makes such heterojunctions an attractive proposition for low-cost optoelectronics. Whilst the limited diffusion length of the organic molecules investigated herein limits the efficiency of solar cells, one application where a bilayer architecture may be preferable to a mixed-phase architecture is in photodetectors, where minimizing the donor–acceptor interface helps to reduce intra-gap trap states and hence the dark saturation current (J_D).[78] Further, it has been shown that non-radiative recombination dominates J_D in organic photodetectors and limits the

achievable detectivity (D^*).[79] Given the extremely low $\Delta V_{oc,nrad}$ of the CuSCN/Y6 device, this makes this heterojunction a promising candidate for low-noise photodetection and since the absorption spectrum of Y6 spans from 650 to 950 nm (Figure S9, Supporting Information), this additionally gives the possibility of NIR photodetection, which is widely used in medical, industrial, or communication settings.[80]

Figure 4A thus shows the J–V characteristics of a CuSCN/Y6-based photodetector in the dark, with the same device structure as used for the fabricated PV devices but with an increased Y6 thickness of 100 nm in order to decrease shunt currents. The device shows very low dark current densities of 0.04, 5, and 10 nA cm^{-2} at applied voltages of 0, −0.5, and −2 V, respectively, which are amongst the lowest reported for organic-semiconductor-based photodetectors.[81,82] Since there is only a small sacrifice in photocurrent in this thicker device compared to the optimized device (Figure S11, Supporting Information) the on/off ratio of the device at AM1.5 illumination is over 8 orders of magnitude at zero bias and over 6 orders of magnitude at reverse biases up to −2 V. Such low J_D values are on par with the best performing organic NIR BHJ photodetectors and suggest a low density of intra-gap trap states,[78] reiterating that the CuSCN/organic interface is not a major source of trap states as is the case at other hybrid heterojunctions.[8]
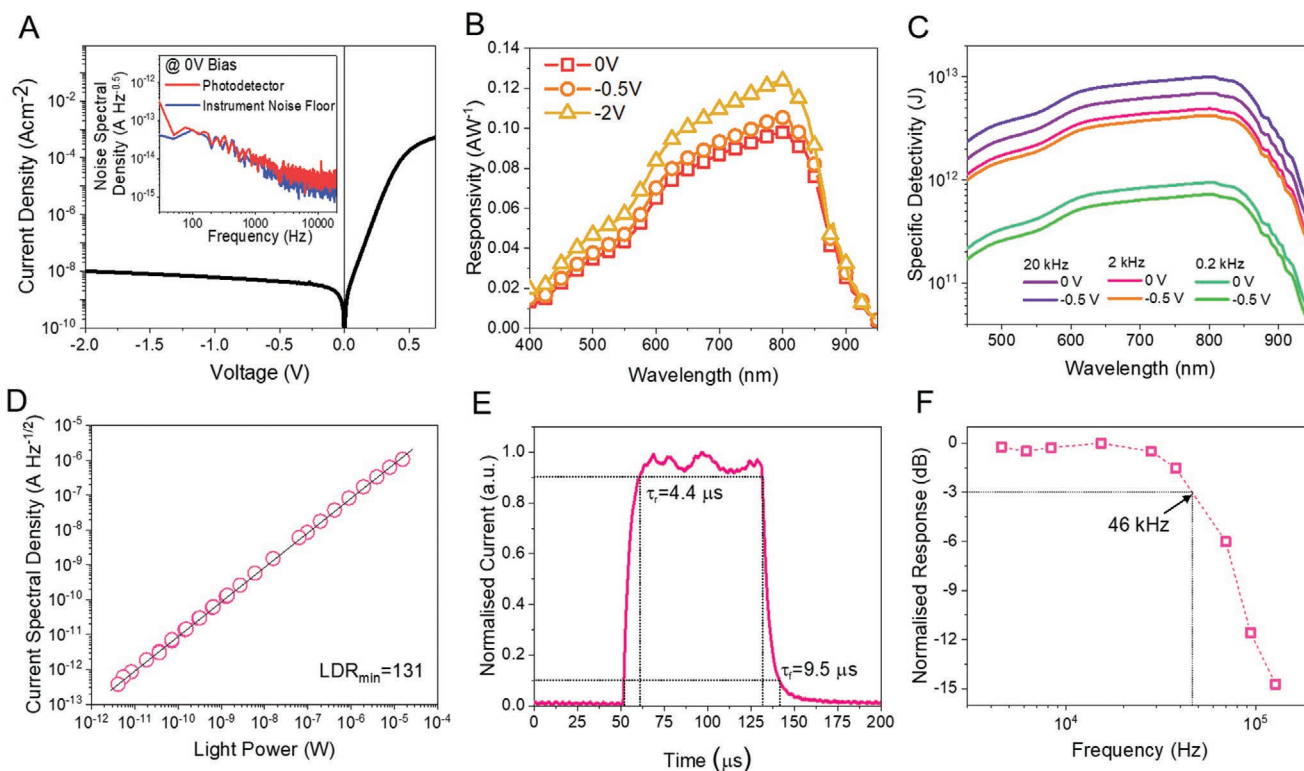

Figure 4. A) Current-density against voltage plot in the dark of a CuSCN/Y6 photodetector. The inset shows the measured noise spectral density for the same device (red line) as a function of frequency, and the noise floor of our experimental set-up (blue line). B) Responsivity of the same device measured at different applied biases. C) Specific detectivity calculated from the responsivity and the noise spectral density at frequencies of 20, 2, and 0.2 kHz at no applied bias and at −0.5 V applied bias. D) Measured current spectral density at 200 Hz at different incident light powers at a wavelength of 830 nm, with a linear fit to the data showing a minimum LDR of 131. E) Transient photocurrent response of the photodetector under a 80 µs pulse at a wavelength of 830 nm. The rise (τ_r) and fall (τ_f) times, calculated by the time it takes for the current to rise (fall) from 10 (90) to 90% (10%) of the plateau current. F) Photocurrent response normalized to the photocurrent at continuous illumination as a function of frequency, showing the −3 dB cut-off frequency at 46 kHz.

**ADVANCED
SCIENCE NEWS**

www.advancedsciencenews.com

**ADVANCED
MATERIALS**

www.advmat.de

The reverse dark current is the major contributor to the shot noise, but an accurate description of the noise current must also include contributions to the thermal and flicker noise as a function of the frequency response.[83] The inset in Figure 4A thus shows the noise spectral density, i_n, obtained by a fast Fourier transform of the dark current as a function of time, in a frequency range from 30 Hz to 30 kHz of the CuSCN/Y6 photodetector (red line) at zero applied bias and the noise floor of our measurement set-up (blue line). Below ≈2 kHz the noise current of the photodetector is limited by the noise floor of our measurement set-up, whilst beyond 2 kHz the noise current tends toward ≈4 fA Hz$^{-0.5}$. Similarly low noise current were obtained at low negative applied voltages, with a small increase in the noise current observed starting from –1 V (Figure S12, Supporting Information). Again, such low noise currents are amongst the lowest reported for any thin-film photodetector technology.

In order to measure the response of the photodetector under illumination, we calculated the responsivity, R from the measured EQE spectrum (Figure S13, Supporting Information), via $R = EQE \times e/h\nu$, and which is shown in Figure 4B at different applied biases. R peaks at a wavelength of ≈810 nm, reaching 0.10 and 0.12 AW^{-1} at 0 and –2 V applied bias, respectively, making the device suitable for NIR light detection. Using the measured responsivity and noise current, the specific detectivity (D^*) can be calculated from the noise equivalent power (NEP) via

$$D^* = \frac{\sqrt{AB}}{(NEP)} = \frac{R\sqrt{AB}}{i_n} \tag{1}$$

where A is the detector area and B is the electric bandwidth. As shown in Figure 4C, the highest D^* value is achieved at a small reverse bias of –0.5 V, reaching 9.97×10^{12} Jones at a wavelength of 810 nm, at a frequency of 20 kHz, with a slightly lower value of 6.67×10^{12} Jones achieved at zero applied bias at the same frequency. Such high values of D^* suggest that the light detection limit of the photodetector (the NEP) can reach 2×10^{-14} W Hz$^{1/2}$ via Equation (1), and is therefore amongst the few reported cases of organic-semiconductor-based photodetectors that allow NIR light detection of sub-picowatt signals.[81] At 2 kHz, D^* is around half that achieved at 20 kHz, and is even lower at 0.2 kHz (< 10^{12} Jones), although it should be noted that at such low frequencies the noise current of the photodetector reaches the noise floor of our experimental set-up and that this therefore sets a lower bound for D^* at these frequencies. The specific detectivities at a greater reverse bias of –2 V (Figure S14, Supporting Information) are slightly lower still, but still reach >10^{12} Jones at frequencies above 2 kHz. The herein measured values of D^* are amongst the highest, if not the highest, recorded for NIR organic or perovskite thin-film photodetectors[81] and approach those achieved by silicon photodetectors.[79]

We additionally measured the linearity of the light response at low light intensities by recording the current response under decreasing light intensity at a specific frequency, as shown in Figure S15, Supporting Information.[84,85] As observed in Figure 4D, at a wavelength of 830 nm and zero applied bias and a frequency of 200 Hz, the photoresponse of the detector is linear down to the lowest light power (4×10^{-12} W) available within our set-up, and approaches the NEP calculated above

using the measured dark noise spectral density and responsivity at this frequency (4×10^{-13} W). This directly validates the high specific detectivities calculated above. We also note that the measured current is linear across the whole light-power range available to us (over 7 orders of magnitude), leading to a minimum linear-dynamic-range (LDR) of 131.

Finally, we also measured the time-dependent response of the photodetector. Figure 4E shows the photocurrent response of the device in response to a 80 µs light pulse at a wavelength of 830 nm at no applied bias. From the photodetector response a rise time t_r (time for which device response rises from 10 to 90%) and a fall time t_f (time for which sensor response decreases from 90 to 10%) of 4.4 and 9.5 µs, respectively, was measured. Such response speed values are typical of organic or perovskite photodetectors measured at no external bias.[81,86–88] Further, the temporal response at various light intensity modulation frequencies was measured, with the maximum recorded photocurrent (in decibel normalized to the photocurrent as 0 Hz) plotted against frequency in Figure 4F. The cut-off frequency, defined as the frequency at which the output of the photodetector is attenuated to –3 dB (70.8% of the original photocurrent), is calculated to be 42 kHz, which defines the applicable bandwidth of the photodetector. This cut-off frequency is similar to comparable OPDs and is fast enough for applications such as medical monitoring and image sensors.[80,81,89]

5. Conclusion

We have demonstrated the first instances of CT state formation between an inorganic p-type semiconductor (CuSCN) and various n-type organic semiconductors through measurements of tail-state EQE and EL spectra. Contrary to previous reports for inorganic–organic heterojunctions, we demonstrate that photogenerated excitons in the organic semiconductor can be effectively converted into free charges through the mediation of CT states. This allows for the fabrication of simple and potentially low cost planar organic solar cells with extremely low non-radiative voltage losses (0.21 V) and photodetectors with low dark current (40 pA cm^{-2}) and noise spectral density (3 fA Hz$^{-1/2}$) at no external bias in CuSCN/Y6 devices. As a result, we measure specific detectivities of just under 10^{13} Jones at NIR wavelengths, which are amongst the highest reported for organic or hybrid photodetectors and allow for NIR light detection of sub-picowatt signals (2×10^{-14} W). We finally show that such photodetectors show a temporal response to NIR illumination in the low microsecond timescale at no external bias and a –3 dB cut-off frequency of 42 kHz. We thus believe that the presented work re-opens the door to exploring hybrid heterojunctions for optoelectronic devices that can exploit the unique property of combining low-cost transparent inorganic materials with color-tunable organic semiconductors

Supporting Information

Supporting Information is available from the Wiley Online Library or from the author.

Conflict of Interest

The authors declare no conflict of interest.

Data Availability Statement

The data that support the findings of this study are available from the corresponding author upon reasonable request.

[1] S.-S. Li, C.-W. Chen, *J. Mater. Chem. A* **2013**, *1*, 10574.
[2] X. Fan, M. Zhang, X. Wang, F. Yang, X. Meng, *J. Mater. Chem. A* **2013**, *1*, 8694.
[3] N. Bansal, L. X. Reynolds, A. MacLachlan, T. Lutz, R. S. Ashraf, W. Zhang, C. B. Nielsen, I. McCulloch, D. G. Rebois, T. Kirchartz, M. S. Hill, K. C. Molloy, J. Nelson, S. A. Haque, *Sci. Rep.* **2013**, *3*, 1531.
[4] C. K. Renshaw, S. R. Forrest, *Phys. Rev. B* **2014**, *90*, 045303.
[5] K. M. Noone, S. Subramaniyan, Q. Zhang, G. Cao, S. A. Jenekhe, D. S. Ginger, *J. Phys. Chem. C* **2011**, *115*, 24403.
[6] J. Chandrasekaran, D. Nithyaprakash, K. B. Ajjan, S. Maruthamuthu, D. Manoharan, S. Kumar, *Renewable Sustainable Energy Rev.* **2011**, *15*, 1228.
[7] S. Günes, N. S. Sariciftci, *Inorg. Chim. Acta* **2008**, *361*, 581.
[8] A. Panda, C. K. Renshaw, A. Oskooi, K. Lee, S. R. Forrest, *Phys. Rev. B* **2014**, *90*, 045302.
[9] M. Eyer, J. Frisch, S. Sadofev, N. Koch, E. J. W. List-Kratochvil, S. Blumstengel, *J. Phys. Chem. C* **2017**, *121*, 21955.
[10] A. Panda, K. Ding, X. Liu, S. R. Forrest, *Phys. Rev. B* **2016**, *94*, 125429.
[11] H. Li, J. L. Bredas, *Adv. Mater.* **2015**, *28*, 3928.
[12] U. B. Cappel, S. A. Dowland, L. X. Reynolds, S. Dimitrov, S. A. Haque, *J. Phys. Chem. Lett.* **2013**, *4*, 4253.
[13] Y. Cai, L. Tang, J. Xiang, R. Ji, S. K. Lai, S. P. Lau, J. Zhao, J. Kong, K. Zhang, *Appl. Phys. Lett.* **2016**, *109*, 073103.
[14] Y. Sevinchan, P. E. Hopkinson, A. A. Bakulin, J. Herz, M. Motzkus, Y. Vaynzof, *Adv. Mater. Interfaces* **2016**, *3*, 1500616.
[15] J. Yuan, Y. Zhang, L. Zhou, G. Zhang, H.-L. Yip, T.-K. Lau, X. Lu, C. Zhu, H. Peng, P. A. Johnson, M. Leclerc, Y. Cao, J. Ulanski, Y. Li, Y. Zou, *Joule* **2019**, *3*, 1140.
[16] M. Wright, A. Uddin, *Sol. Energy Mater. Sol. Cells* **2012**, *107*, 87.
[17] S. Dowland, T. Lutz, A. Ward, S. P. King, A. Sudlow, M. S. Hill, K. C. Molloy, S. A. Haque, *Adv. Mater.* **2011**, *23*, 2739.
[18] H. C. Leventis, S. P. King, A. Sudlow, M. S. Hill, K. C. Molloy, S. A. Haque, *Nano Lett.* **2010**, *10*, 1253.
[19] T. Rath, D. Scheunemann, R. Canteri, H. Amenitsch, J. Handl, K. Wewerka, G. Kothleitner, S. Leimgruber, A.-C. Knall, S. A. Haque, *J. Mater. Chem. C* **2019**, *7*, 943.
[20] K. Matras-Postołek, A. Żaba, E. M. Nowak, P. Dąbczyński, J. Rysz, J. Sanetra, *Appl. Surf. Sci.* **2018**, *451*, 180.
[21] D. Ding, T. Rath, L. Lanzetta, J. Manuel Marin-Beloqui, S. A. Haque, *ACS Appl. Energy Mater.* **2018**, *1*, 3042.
[22] F. Piersimoni, R. Schlesinger, J. Benduhn, D. Spoltore, S. Reiter, I. Lange, N. Koch, K. Vandewal, D. Neher, *J. Phys. Chem. Lett.* **2015**, *6*, 500.
[23] Y. Vaynzof, A. A. Bakulin, S. Gélinas, R. H. Friend, *Phys. Rev. Lett.* **2012**, *108*, 246605.
[24] G. Wu, Z. Li, X. Zhang, G. Lu, *J. Phys. Chem. Lett.* **2014**, *5*, 2649.
[25] R. Tang, S. Han, F. Teng, K. Hu, Z. Zhang, M. Hu, X. Fang, *Adv. Sci.* **2018**, *5*, 1700334.
[26] A. Pickett, A. Mohapatra, A. Laudari, S. Khanra, T. Ram, S. Patil, S. Guha, *Org. Electron.* **2017**, *45*, 115.
[27] S. A. Dowland, L. X. Reynolds, A. MacLachlan, U. B. Cappel, S. A. Haque, *J. Mater. Chem. A* **2013**, *1*, 13896.
[28] R. Zhou, R. Stalder, D. Xie, W. Cao, Y. Zheng, Y. Yang, M. Plaisant, P. H. Holloway, K. S. Schanze, J. R. Reynolds, J. Xue, *ACS Nano* **2013**, *7*, 4846.
[29] X. Wang, W. Song, B. Liu, G. Chen, D. Chen, C. Zhou, G. Shen, *Adv. Funct. Mater.* **2013**, *23*, 1202.
[30] K. Tvingstedt, K. Vandewal, A. Gadisa, F. Zhang, J. Manca, O. Inganäs, *J. Am. Chem. Soc.* **2009**, *131*, 11819.
[31] I. Haeldermans, K. Vandewal, W. D. Oosterbaan, A. Gadisa, J. D'Haen, M. K. Van Bael, J. V. Manca, J. Mullens, *Appl. Phys. Lett.* **2008**, *93*, 223302.
[32] K. Vandewal, A. Gadisa, W. D. Oosterbaan, S. Bertho, F. Banishoeib, I. Van Severen, L. Lutsen, T. J. Cleij, D. Vanderzande, J. V. Manca, *Adv. Funct. Mater.* **2008**, *18*, 2064.
[33] A. Panda, S. R. Forrest, *Nano Lett.* **2017**, *17*, 7853.
[34] Y. Firdaus, V. M. Le Corre, S. Karuthedath, W. Liu, A. Markina, W. Huang, S. Chattopadhyay, M. M. Nahid, M. I. Nugraha, Y. Lin, A. Seitkhan, A. Basu, W. Zhang, I. McCulloch, H. Ade, J. Labram, F. Laquai, D. Andrienko, L. J. A. Koster, T. D. Anthopoulos, *Nat. Commun.* **2020**, *11*, 5220.
[35] S. Karuthedath, J. Gorenflot, Y. Firdaus, W.-Y. Sit, F. Eisner, A. Seitkhan, M. K. Ravva, T. D. Anthopoulos, F. Laquai, *Adv. Energy Mater.* **2019**, *9*, 1802476.
[36] W. Y. Sit, F. D. Eisner, Y. H. Lin, Y. Firdaus, A. Seitkhan, A. H. Balawi, F. Laquai, C. H. Burgess, M. A. McLachlan, G. Volonakis, F. Giustino, T. D. Anthopoulos, *Adv. Sci.* **2018**, *5*, 1700980.
[37] Y. Firdaus, A. Seitkhan, F. Eisner, W. Y. Sit, Z. Kan, N. Wehbe, A. H. Balawi, E. Yengel, S. Karuthedath, F. Laquai, T. D. Anthopoulos, *Sol. RRL* **2018**, *2*, 1800095.
[38] C. Yan, S. Barlow, Z. Wang, H. Yan, A. K. Y. Jen, S. R. Marder, X. Zhan, *Nat. Rev. Mater.* **2018**, *3*, 18003.
[39] W. Zhao, D. Qian, S. Zhang, S. Li, O. Inganäs, F. Gao, J. Hou, *Adv. Mater.* **2016**, *28*, 4734.
[40] Y. Lin, J. Wang, Z.-G. Zhang, H. Bai, Y. Li, D. Zhu, X. Zhan, *Adv. Mater.* **2015**, *27*, 1170.
[41] F. Eisner, M. Azzouzi, Z. Fei, X. Hou, T. D. Anthopoulos, T. J. S. Dennis, M. J. Heeney, J. Nelson, *J. Am. Chem. Soc.* **2019**, *141*, 6362.
[42] Z. Fei, F. D. Eisner, X. Jiao, M. Azzouzi, J. A. Röhr, Y. Han, M. Shahid, A. S. R. Chesman, C. D. Easton, C. R. McNeill, T. D. Anthopoulos, J. Nelson, M. Heeney, *Adv. Mater.* **2018**, *30*, 1705209.
[43] H. Jiang, Z. Wang, L. Zhang, A. Zhong, X. Liu, F. Pan, W. Cai, O. Inganäs, Y. Liu, J. Chen, Y. Cao, *ACS Appl. Mater. Interfaces* **2017**, *9*, 36061.

**ADVANCED
SCIENCE NEWS**

www.advancedsciencenews.com

**ADVANCED
MATERIALS**

www.advmat.de

[44] U. Hörmann, S. Zeiske, F. Piersimoni, L. Hoffmann, R. Schlesinger, N. Koch, T. Riedl, D. Andrienko, D. Neher, *Phys. Rev. B* **2018**, *98*, 155312.

[45] K. Vandewal, K. Tvingstedt, A. Gadisa, O. Inganäs, J. V. Manca, *Phys. Rev. B* **2010**, *81*, 125204.

[46] S. Karuthedath, J. Gorenflot, Y. Firdaus, N. Chaturvedi, C. S. P. De Castro, G. T. Harrison, J. I. Khan, A. Markina, A. H. Balawi, T. A. D. Peña, W. Liu, R.-Z. Liang, A. Sharma, S. H. K. Paleti, W. Zhang, Y. Lin, E. Alarousu, D. H. Anjum, P. M. Beaujuge, S. De Wolf, I. McCulloch, T. D. Anthopoulos, D. Baran, D. Andrienko, F. Laquai, *Nat. Mater.* **2021**, *20*, 378.

[47] H. Lim, H. Kwon, S. K. Kim, J. W. Kim, *J. Phys. Chem. Lett.* **2017**, *8*, 4763.

[48] H. Li, J.-L. Bredas, *Adv. Mater.* **2016**, *28*, 3928.

[49] S. Yunus, P. E. Hopkinson, A. A. Bakulin, H. Julia, M. Marcus, V. Yana, *Adv. Mater. Interfaces* **2016**, *3*, 1500616.

[50] A. Grupp, P. Ehrenreich, J. Kalb, A. Budweg, L. Schmidt-Mende, D. Brida, *J. Phys. Chem. Lett.* **2017**, *8*, 4858.

[51] H. Lu, J. Joy, R. L. Gaspar, S. E. Bradforth, R. L. Brutchey, *Chem. Mater.* **2016**, *28*, 1897.

[52] G. F. Burkhard, E. T. Hoke, M. D. McGehee, *Adv. Mater.* **2010**, *22*, 3293.

[53] M. A. Faist, T. Kirchartz, W. Gong, R. S. Ashraf, I. McCulloch, J. C. de Mello, N. J. Ekins-Daukes, D. D. C. Bradley, J. Nelson, *J. Am. Chem. Soc.* **2012**, *134*, 685.

[54] E. Collado-Fregoso, S. N. Pugliese, M. Wojcik, J. Benduhn, E. Bar-Or, L. Perdigon Toro, U. Hörmann, D. Spoltore, K. Vandewal, J. M. Hodgkiss, D. Neher, *J. Am. Chem. Soc.* **2019**, *141*, 2329.

[55] B. P. Rand, D. P. Burk, S. R. Forrest, *Phys. Rev. B* **2007**, *75*, 115327.

[56] H.-S. Lin, I. Jeon, R. Xiang, S. Seo, J.-W. Lee, C. Li, A. Pal, S. Manzhos, M. S. Goorsky, Y. Yang, S. Maruyama, Y. Matsuo, *ACS Appl. Mater. Interfaces* **2018**, *10*, 39590.

[57] W. Zhang, J. Huang, J. Xu, M. Han, D. Su, N. Wu, C. Zhang, A. Xu, C. Zhan, *Adv. Energy Mater.* **2020**, *10*, 2001436.

[58] W. Li, W. Liu, X. Zhang, D. Yan, F. Liu, C. Zhan, *Macromol. Rapid Commun.* **2019**, *40*, 1900353.

[59] H. Raboui, E. S. Thibau, D. S. Josey, Z.-H. Lu, T. P. Bender, *J. Mater. Chem. A* **2017**, *5*, 10978.

[60] Q. Burlingame, X. Huang, X. Liu, C. Jeong, C. Coburn, S. R. Forrest, *Nature* **2019**, *573*, 394.

[61] Q. Burlingame, C. Coburn, X. Che, A. Panda, Y. Qu, S. R. Forrest, *Nature* **2018**, *554*, 77.

[62] J. Yao, T. Kirchartz, M. S. Vezie, M. A. Faist, W. Gong, Z. He, H. Wu, J. Troughton, T. Watson, D. Bryant, J. Nelson, *Phys. Rev. Appl.* **2015**, *4*, 014020.

[63] J. Benduhn, K. Tvingstedt, F. Piersimoni, S. Ullbrich, Y. Fan, M. Tropiano, K. A. McGarry, O. Zeika, M. K. Riede, C. J. Douglas, S. Barlow, S. R. Marder, D. Neher, D. Spoltore, K. Vandewal, *Nat. Energy* **2017**, *2*, 17053.

[64] R. Englman, J. Jortner, *Mol. Phys.* **1970**, *18*, 145.

[65] Y. Cui, H. Yao, J. Zhang, T. Zhang, Y. Wang, L. Hong, K. Xian, B. Xu, S. Zhang, J. Peng, Z. Wei, F. Gao, J. Hou, *Nat. Commun.* **2019**, *10*, 2515.

[66] S. Liu, J. Yuan, W. Deng, M. Luo, Y. Xie, Q. Liang, Y. Zou, Z. He, H. Wu, Y. Cao, *Nat. Photonics* **2020**, *14*, 300.

[67] Y. Wang, D. Qian, Y. Cui, H. Zhang, J. Hou, K. Vandewal, T. Kirchartz, F. Gao, *Adv. Energy Mater.* **2018**, *8*, 1801352.

[68] G. Zhang, X.-K. Chen, J. Xiao, P. C. Y. Chow, M. Ren, G. Kupgan, X. Jiao, C. C. S. Chan, X. Du, R. Xia, Z. Chen, J. Yuan, Y. Zhang, S. Zhang, Y. Liu, Y. Zou, H. Yan, K. S. Wong, V. Coropceanu, N. Li, C. J. Brabec, J.-L. Bredas, H.-L. Yip, Y. Cao, *Nat. Commun.* **2020**, *11*, 3943.

[69] X.-K. Chen, D. Qian, Y. Wang, T. Kirchartz, W. Tress, H. Yao, J. Yuan, M. Hülsbeck, M. Zhang, Y. Zou, Y. Sun, Y. Li, J. Hou, O. Inganäs, V. Coropceanu, J.-L. Bredas, F. Gao, *Nat. Energy* **2021**, *6*, 799.

[70] M. Azzouzi, J. Yan, T. Kirchartz, K. Liu, J. Wang, H. Wu, J. Nelson, *Phys. Rev. X* **2018**, *8*, 031055.

[71] P. Pattanasattayavong, V. Promarak, T. D. Anthopoulos, *Adv. Electron. Mater.* **2017**, *3*, 1600378.

[72] J. E. Jaffe, T. C. Kaspar, T. C. Droubay, T. Varga, M. E. Bowden, G. J. Exarhos, *J. Phys. Chem. C* **2010**, *114*, 9111.

[73] P. Pattanasattayavong, N. Yaacobi-Gross, K. Zhao, G. O. Ndjawa, J. Li, F. Yan, B. C. O'Regan, A. Amassian, T. D. Anthopoulos, *Adv. Mater.* **2013**, *25*, 1504.

[74] T. Leonidas, *J. Phys.: Condens. Matter* **2016**, *28*, 295801.

[75] P. Pattanasattayavong, A. D. Mottram, F. Yan, T. D. Anthopoulos, *Adv. Funct. Mater.* **2015**, *25*, 6802.

[76] Sigma-Aldrich Copper(I) Thiocyanate (250 g). https://www.sigmaaldrich.com/catalog/product/aldrich/298212 (accessed: August 2020).

[77] Osilla Regioregular poly(3-hexylthiophene-2,5-diyl) https://www.ossila.com/products/p3ht?variant=18448157343840 (accessed: August 2020).

[78] J. Kublitski, A. Hofacker, B. K. Boroujeni, J. Benduhn, V. C. Nikolis, C. Kaiser, D. Spoltore, H. Kleemann, A. Fischer, F. Ellinger, K. Vandewal, K. Leo, *Nat. Commun.* **2021**, *12*, 551.

[79] S. Gielen, C. Kaiser, F. Verstraeten, J. Kublitski, J. Benduhn, D. Spoltore, P. Verstappen, W. Maes, P. Meredith, A. Armin, K. Vandewal, *Adv. Mater.* **2020**, *32*, 2003818.

[80] A. Armin, R. D. Jansen-van Vuuren, N. Kopidakis, P. L. Burn, P. Meredith, *Nat. Commun.* **2015**, *6*, 6343.

[81] J. Huang, J. Lee, J. Vollbrecht, V. V. Brus, A. L. Dixon, D. X. Cao, Z. Zhu, Z. Du, H. Wang, K. Cho, G. C. Bazan, T.-Q. Nguyen, *Adv. Mater.* **2020**, *32*, 1906027.

[82] P. C. Y. Chow, T. Someya, *Adv. Mater.* **2020**, *32*, 1902045.

[83] Y. Fang, A. Armin, P. Meredith, J. Huang, *Nat. Photonics* **2019**, *13*, 1.

[84] Y. Fang, J. Huang, *Adv. Mater.* **2015**, *27*, 2804.

[85] L. Zhang, T. Yang, L. Shen, Y. Fang, L. Dang, N. Zhou, X. Guo, Z. Hong, Y. Yang, H. Wu, J. Huang, Y. Liang, *Adv. Mater.* **2015**, *27*, 6496.

[86] J. Wang, S. Xiao, W. Qian, K. Zhang, J. Yu, X. Xu, G. Wang, S. Zheng, S. Yang, *Adv. Mater.* **2021**, *33*, 2005557.

[87] W. Li, Y. Xu, X. Meng, Z. Xiao, R. Li, L. Jiang, L. Cui, M. Zheng, C. Liu, L. Ding, Q. Lin, *Adv. Funct. Mater.* **2019**, *29*, 1808948.

[88] Y. Zhao, Y. Qiu, H. Gao, J. Feng, G. Chen, L. Jiang, Y. Wu, *Adv. Mater.* **2020**, *32*, 1905298.

[89] M. Biele, C. Montenegro Benavides, J. Hürdler, S. F. Tedde, C. J. Brabec, O. Schmidt, *Adv. Mater. Technol.* **2019**, *4*, 1800158.

2104654 (9 of 9)